JOURNAL OF MATERIALS SCIENCE **36** (2001) 703–713

Change in bulk and surface structure of mixed MoO_3-ZnO oxide by heat treatment in air and in hydrogen

NORIYUKI SOTANI, TAKASHI SUZUKI, KENTARO NAKAMURA, KAZUO EDA
Department of Chemistry, Faculty of Science, Kobe University, Nada, Kobe, 657-8501, Japan
E-mail: sotani@kobe-u.ac.jp

SADAO HASEGAWA
Department of Chemistry, Tokyo Gakugei University, Koganei-shi, Tokyo 184-0015, Japan

The mixed MoO_3-ZnO oxides with various mole fraction of Mo, X_{Mo}, obtained by the impregnation method were heated in air and in hydrogen. As for the mixed oxide heated in air, MoO_3 reacted stoichiometrically with ZnO to give $ZnMoO_4$ at $X_{Mo} < 0.5$, while at $X_{Mo} > 0.5$, the reaction did not proceed completely. On the other hand, for the mixed oxide heated in hydrogen, at $X_{Mo} < 0.5$ $ZnMoO_4$ was reduced to $ZnMoO_3$ with the anion vacancy, while at $X_{Mo} > 0.5$, MoO_3 was reduced to MoO_2 and $ZnMoO_4$ was difficult to be reduced to $ZnMoO_3$. The structure of the surface and/or near the surface was different from the bulk structure.

1. Introduction

Supported molybdenum oxide catalysts are widely used in various catalytic processes [1]. The structure of the supported molybdenum oxide species is depended a function of the specific support, the extent of surface hydration and dehydration, the surface molybdenum oxide coverage, the surface impurity, and the calcination temperature [2–5]. Most of molybdenum oxides are supported on Al_2O_3 [6, 7], SiO_2 [8, 9], TiO_2 [10, 11], ZrO_2 [12, 13], and Nb_2O_5 [14, 15]. Usually the reaction between MoO_3 and the support did not take place [16].

On the other hand, in the case of MoO_3 supported on MgO, most of Mo ions are thought to be stabilized in a tetrahedral MoO_4 unit of the magnesium molybdate ($MgMoO_4$) phase formed by calcination [17–19]. Aritani *et al.* [20, 21] studied the structure of the mixed MoO_3-MgO oxide by changing the Mo/Mg ratio and found that when the binary MoO_3-MgO oxide was calcined in air the reaction between MoO_3 and MgO took place to give a mixture of MgO and α-$MgMoO_4$ at low Mo/Mg ratio, and of MoO_3 and $Mg_2Mo_3O_{11}$ at high Mo/Mg ratio. By reduction with hydrogen MoO_2 appeared on the surface.

ZnO is well known [22–24] to be a n-type semiconductor and is applied as a photo chemical device. Therefore, the mixed MoO_3-ZnO oxide is expected to give a new catalytic function. Nakamura *et al.* [25] found the catalytic activity for 1-butene isomerization on the mixed MoO_3-ZnO oxide, which was obtained by the impregnation method. However, the composition and structure, and the surface structure of the MoO_3-ZnO mixed oxide had not been so much studied. Therefore, we prepared the mixed MoO_3-ZnO oxide by the impregnation method and treated them at 673 K in air and in hydrogen atmosphere, and studied the difference in the composition and structure of the mixed MoO_3-ZnO oxide by the treatment in air and in hydrogen. In both cases, the solid state reaction took place. We will discuss the difference in the composition and structure of the bulk and the surface.

2. Experimental

2.1. Preparation of the mixed MoO_3-ZnO oxide

The mixed MoO_3-ZnO oxide (denoted as Mo-Zn oxide) was prepared by the usual impregnation technique. Zinc oxide (Sakai Kagaku), ZnO, calcined in air at 673 K for 1 h was suspended at room temperature in the desired amount of 1 M ammonium paramolybdate (Wako Junyaku) solution (pH = 5.89) and was stirred with ultrasonic wave. After filtration the sample was dried completely in air at 393 K for 24 h. The dried sample was calcined in air at 673 K for 2 h and reduced at 673 K with hydrogen for 2 h. The sample was analyzed by atomic absorption analysis using the 313.26 nm line for Mo and the 213.86 nm line for Zn on a SEIKO INSTRUMENTS SAS 7500A atomic absorption spectrophotometer. Fig. 1 shows the result of analysis which is a good agreement within 0.02 percentage error with the mole fraction in the starting solution.

2.2. Characterization

The Mo-Zn oxide was examined by a powder X-ray diffraction (XRD) method using a RIGAKU RINT 1200 X-ray diffractometer with Cu $K_{\alpha 1}$

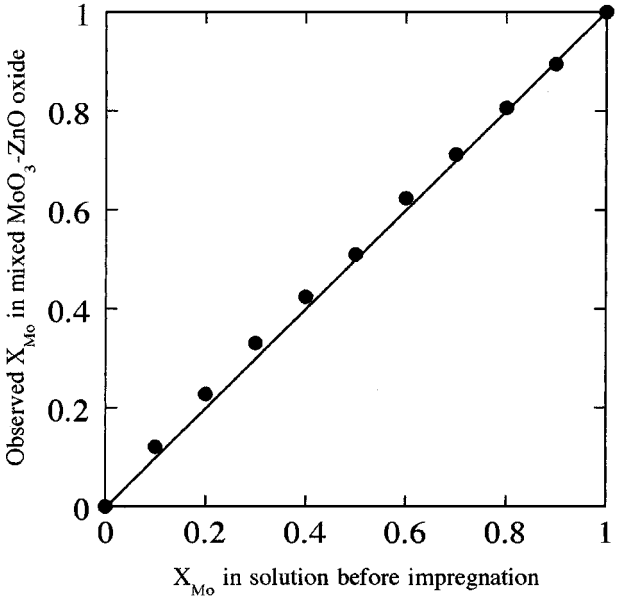

Figure 1 The mole fraction of Mo, X_{Mo}, of the mixed MoO_3-ZnO oxide obtained by the impregnation method. (—) represents the theoretical value and (●), the observed one obtained by an atomic absorption analysis.

($\lambda = 1.45056$ Å) radiation (40 kV, 40 mA). The behavior of paramagnetic species in the oxide was studied by a JEOL TE300 ESR spectrometer with X-band at liquid nitrogen temperature, 77 K. The g-value was determined by using Mn^{2+} marker as a reference. Mo L_3-edge X-ray Absorption Near Edge Structure (XANES) spectrum was measured on BL-7A of UVSOR at Institute of National Laboratory for Molecular Science, Okazaki, Japan, using a Ge (111) two-crystal monochrometer. The spectrum was measured in total electron yield mode at room temperature. Specific surface area (SA, m^2/g) of the Mo-Zn oxide was determined by using a QUANTASORB Jr.

3. Results

3.1. XRD studies of the mixed MoO_3-ZnO oxide

The dried sample after impregnation was studied by XRD, which showed the mixture of $(NH_4)_6Mo_7O_{26}$ and ZnO at X_{Mo} (mole fraction of Mo) $\geqq 0.5$, and that of an unknown ammonium molybdate and ZnO at $X_{Mo} < 0.5$. The dried samples with various X_{Mo} were heated at 673 K in air for various heating time. There was no large change in intensity of XRD patterns though it was calcined for more than 1 h. Therefore, all the samples were treated for 2 h. XRD patterns of the calcined sample with $X_{Mo} = 0.2$, 0.5, and 0.9 are shown in Fig. 2. XRD pattern of $X_{Mo} = 0.2$, 0.5, and 0.9 consists of the mixture of ZnO and $ZnMoO_4$, of ZnO, $ZnMoO_4$ and MoO_3, and of $ZnMoO_4$, MoO_3 and a trace amount of ZnO, respectively. Fig. 3 shows the change in the relative diffraction intensity ratio, I_i/I_t, of the Mo-Zn oxide, where I_i is the diffraction intensity of each component and I_t, the total intensity of all components. I_{ZnO}/I_t decreased steeply at first from $X_{Mo} = 0.1$ to 0.5 and then gradually decreased to 0 at $X_{Mo} = 1$. I_{ZnMoO4}/I_t increased from $X_{Mo} = 0.1$ to

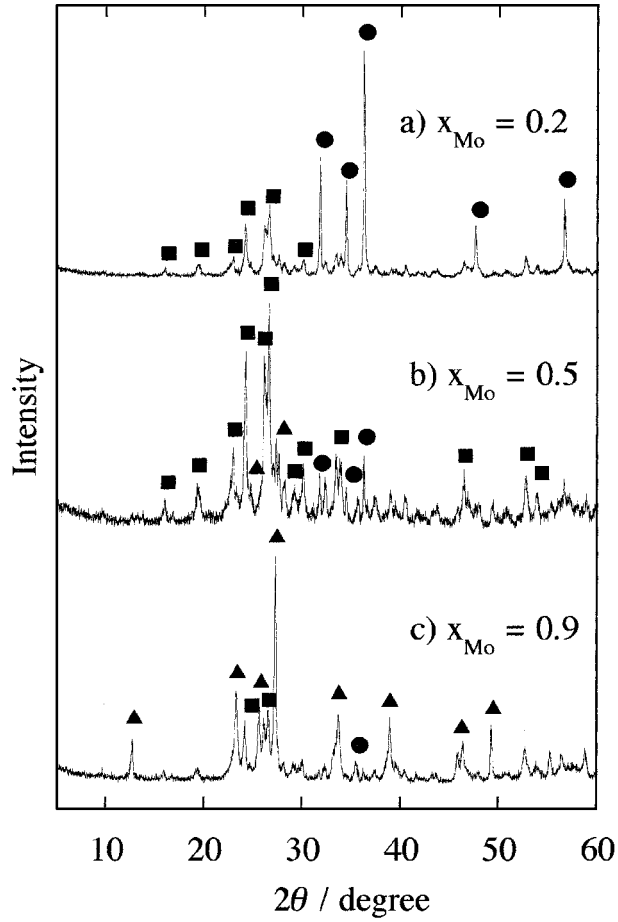

Figure 2 XRD patterns of the mixed MoO_3-ZnO oxide heated in air at 673 K for 2 h; $X_{Mo} =$ (a) 0.2, (b) 0.5, and (c) 0.9. Symbols are (●): ZnO, (■): $ZnMoO_4$, and (▲): MoO_3, respectively.

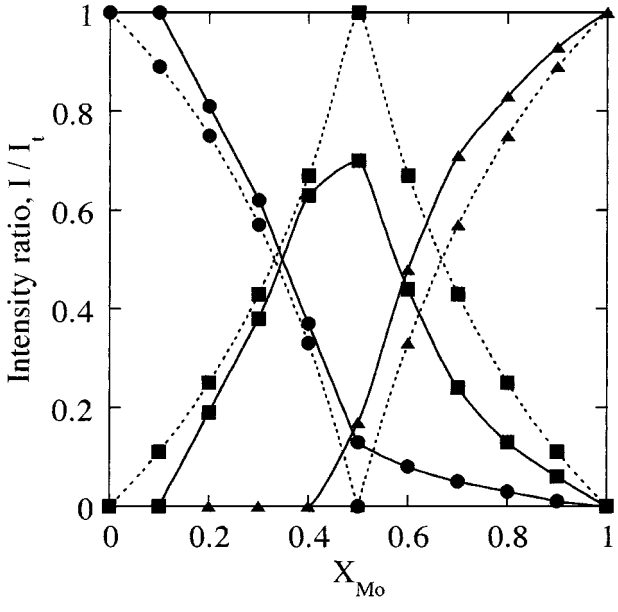

Figure 3 The relative diffraction intensity ratio of the mixed MoO_3-ZnO oxide heated in air at 673 K for 2 h. The solid and dotted lines show the observed and theoretical values, respectively. Symbols are (●): ZnO, (■): $ZnMoO_4$, and (▲): MoO_3., respectively.

0.5, took a maximum at $X_{Mo} = 0.5$, and then decreased with the increase in X_{Mo}. While, I_{MoO3}/I_t increased monotonously from $X_{Mo} = 0.4$ to 1.0. This suggests that MoO_3 and ZnO reacted easily with each other to give $ZnMoO_4$ in solid phase.

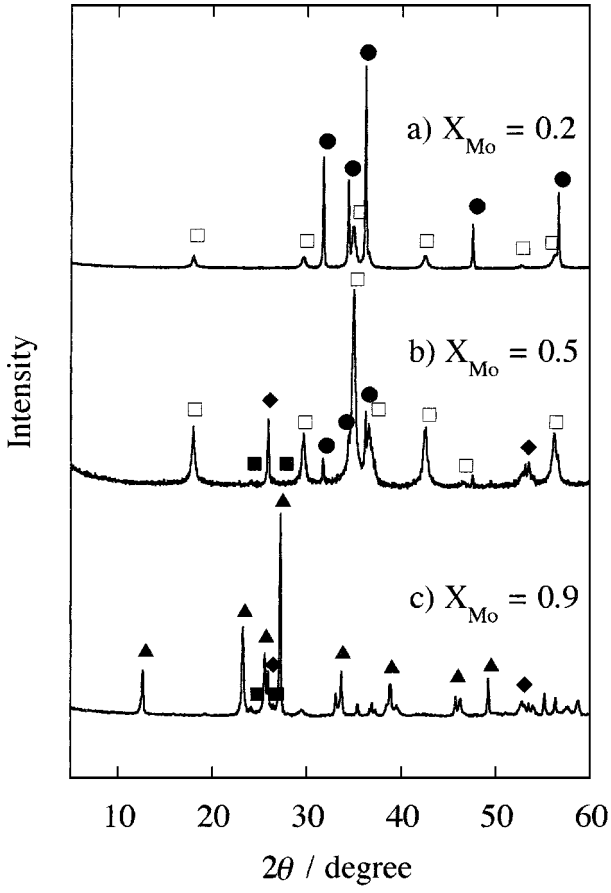

Figure 4 XRD patterns of the mixed MoO_3-ZnO oxide reduced at 673 K with hydrogen for 2 h; X_{Mo} = (a) 0.2, (b) 0.5, and (c) 0.9. Symbols are (●): ZnO, (■): $ZnMoO_4$, (□): $ZnMoO_3$, (♦): MoO_2, and (▲): MoO_3., respectively.

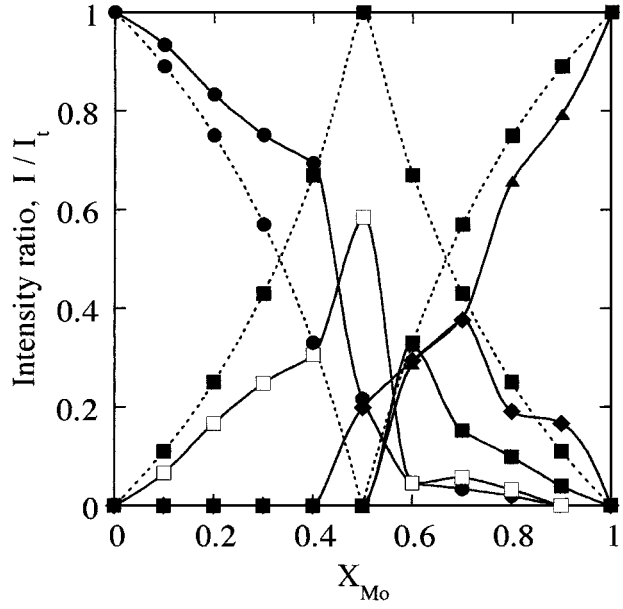

Figure 5 The relative diffraction intensity ratio of the mixed MoO_3-ZnO oxide reduced at 673 K with hydrogen for 2 h. The solid and dotted lines show the observed and theoretical values, respectively. Symbols are (●): ZnO, (■): $ZnMoO_4$, (□): $ZnMoO_3$, (♦): MoO_2, and (▲): MoO_3, respectively.

The Mo-Zn oxide was treated at 673 K with hydrogen for various treating times. There was no large change in XRD pattern of the samples treated for 1–5 h. Fig. 4 shows the XRD pattern of the mixed Mo-Zn oxide reduced at 673 K for 2 h. In addition to ZnO, the new pattern due to $ZnMoO_3$ appeared at $X_{Mo} = 0.2$. At $X_{Mo} = 0.5$, the XRD pattern consisted of four phases of ZnO, $ZnMoO_3$, $ZnMoO_4$, and MoO_2. At $X_{Mo} = 0.9$, the pattern was due to MoO_3, MoO_2, and $ZnMoO_4$. Fig. 5 shows the intensity ratio of each component of the reduced mixed oxide. I_{ZnO}/I_t decreased gradually from $X_{Mo} = 0$ to 0.4, sharply decreased to about 0.05 at $X_{Mo} = 0.6$, and gradually decreased to 0. On the other hand, I_{ZnMoO4}/I_t was 0 from $X_{Mo} = 0$ to 0.5, increased, and took the maximum at $X_{Mo} = 0.6$. At $X_{Mo} = 0.5$, MoO_2 also began to appear. I_{MoO2}/I_t took the maximum at $X_{Mo} = 0.7$, but did not exceed 0.4. We should note that $ZnMoO_3$ and MoO_2 were newly produced in the reduced oxide. These results suggest that $ZnMoO_4$ and MoO_3 were reduced to $ZnMoO_3$ and MoO_2, respectively. However, $X_{Mo} > 0.5$, the reaction process differs from that in the range $X_{Mo} < 0.5$.

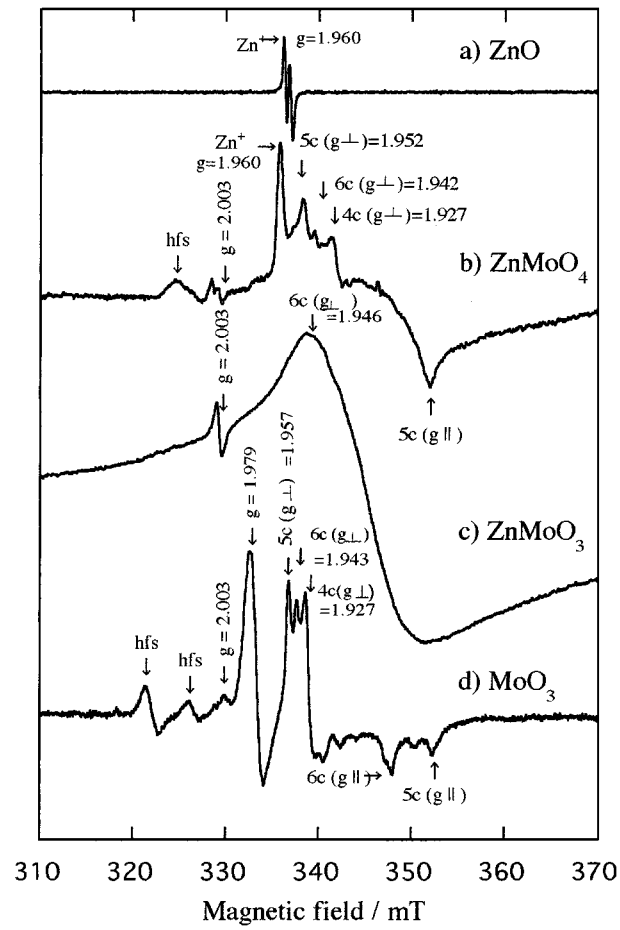

Figure 6 ESR Spectra of (a) ZnO, (b) $ZnMoO_4$, (c) $ZnMoO_3$, and (d) MoO_3 as a standard material.

3.2. ESR studies of the mixed MoO_3-ZnO oxide

ESR study gives us a very important information about the coordination state and the ligand field. Fig. 6 shows ESR spectra of ZnO, $ZnMoO_4$, $ZnMoO_3$, and MoO_3 as a standard material. The ESR spectrum of ZnO gave only a sharp signal at $g = 1.960$, which resulted from Zn^+. $ZnMoO_4$ gave a very complicated signal with $g = 2.003$, 1.960, 1.952, 1.942, 1.927, and 1.874. In

addition, at the lower magnetic field, a hyperfine structure, hfs, was detected. The spectrum of $ZnMoO_3$ was broad and simple with a sharp signal at $g = 2.003$. The g-value at the top of the broad signal was 1.946. The spectrum of MoO_3 as well as $ZnMoO_4$ gave a very complicated spectrum with $g = 1.998$, 1.979, 1.957, 1.943, 1.927, 1.895, and 1.872.

Fig. 7a shows ESR spectra of the mixed Mo-Zn oxide, which are very complicated. Especially, the spectrum of $X_{Mo} = 0.2$ is complicated and gives the peaks at $g = 2.003$, 1.972, 1.960, 1.956, 1.942, 1.927, 1.893, 1.879, and 1.778. The line shape is apparently similar to that of $ZnMoO_4$ as shown in Fig. 6, though the each signal intensity is different. The spectra of $X_{Mo} = 0.5$ and 0.9 give a similar anisotropic line shape. Fig. 7b shows the ESR spectra of the reduced Mo-Zn oxide. At $X_{Mo} = 0.9$, the line shape of the reduced oxide give no significant difference from the unreduced one. However, the line shapes of $X_{Mo} = 0.2$ and 0.5 are simple and differ largely from those of the unreduced one. The spectrum of $X_{Mo} = 0.5$ is very similar to that of $X_{Mo} = 0.2$, but little noisy and no peak at $g = 1.960$.

We tried to assign the g-value obtained in the unreduced and reduced Mo-Zn oxides by considering that of the standard material and the reported g-values [26–34]. ZnO showed only the signal at $g = 1.960$ [30–32], which was assigned to Zn^+. The signal at $g = 2.003$ appeared clearly in the standard $ZnMoO_3$ which possessed the anion vacancy [33] and also appeared in both the unreduced and reduced oxides. According to literatures [26–29], it is assigned to oxygen species and/or lattice defects like anion vacancies. In this case, the active oxygen species can not be formed on the oxide, but it is reasonable that the signal results from the defect such as the anion vacancy.

Another complicated signals should be due to Mo species. Che *et al.* [26] proposed three Mo^{5+} species with tetra-, penta-, and hexa-coordination. According to Che *et al.* and other workers, $g = 1.956$, 1.927, and 1.941–1.943 was assigned to the vertical component ($g \perp$) of the g-value of penta-, tetra-, and hexa-coordinated Mo^{5+} ions [26–29, 34], respectively. The signals at $g = 1.893$, 1.870–1.879, and 1.778 were assigned to the parallel components ($g//$) of the g-value of hexa-, penta-, and tetra-coordinated Mo^{5+} ions, respectively [26–29, 34]. The signal at $g = 1.972$–1.980 [34] was not assigned yet, but this was closely related to the amount of MoO_3 since the signal intensity increased with the increase in the content of MoO_3 in the mixed oxide.

The intensity was determined by comparing the area of the sample with one of the standard Mn^{2+}, which was calculated by integration of the spectrum. The intensity should contain the total amount of the radicals. The relative intensity of the unreduced and reducd Mo-Zn oxide is shown in Fig. 8. At $X_{Mo} = 0.2$ the relative intensity of the reduced Mo-Zn oxide is about five times of that of the unreduced oxide. The dotted line is obtained by subtracting the intensity of the unreduced Mo-Zn oxide from that of the reduced one and clearly shows the increase in the intensity by the reduction. The increase in the intensity is mostly due to Mo^{5+} species, because the intensity due to the defect and Zn^+ ion is assumed

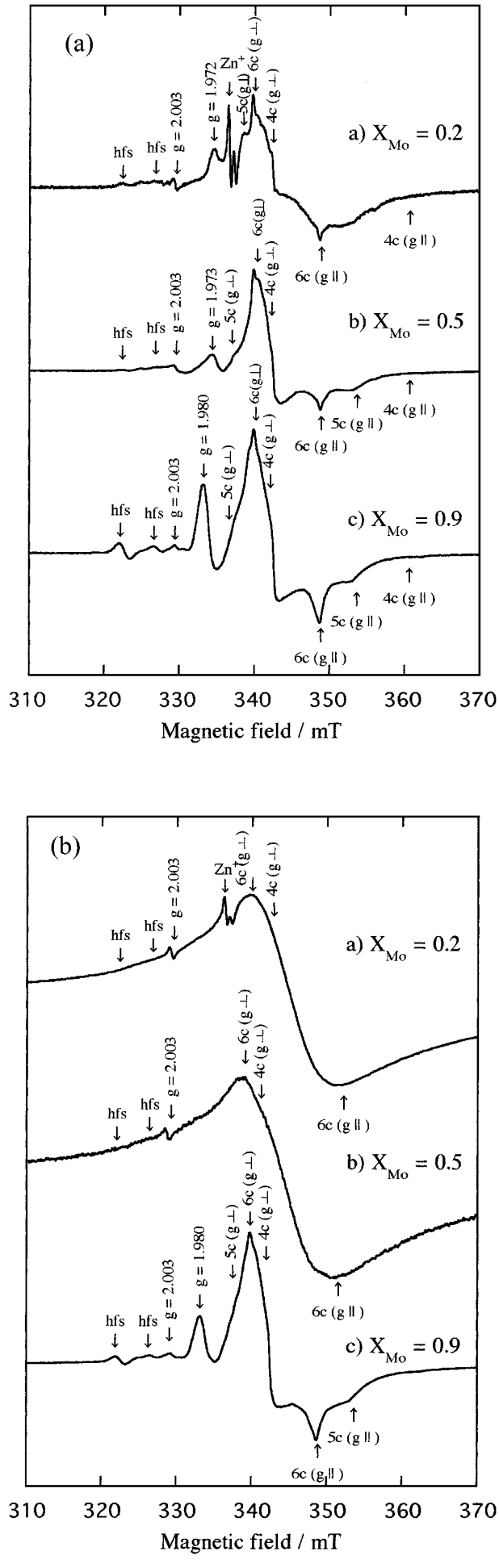

Figure 7 ESR Spectra of the (a) unreduced and (b) reduced MoO_3-ZnO oxide. (a) $X_{Mo} = 0.2$, (b) $X_{Mo} = 0.5$, and (c) $X_{Mo} = 0.9$.

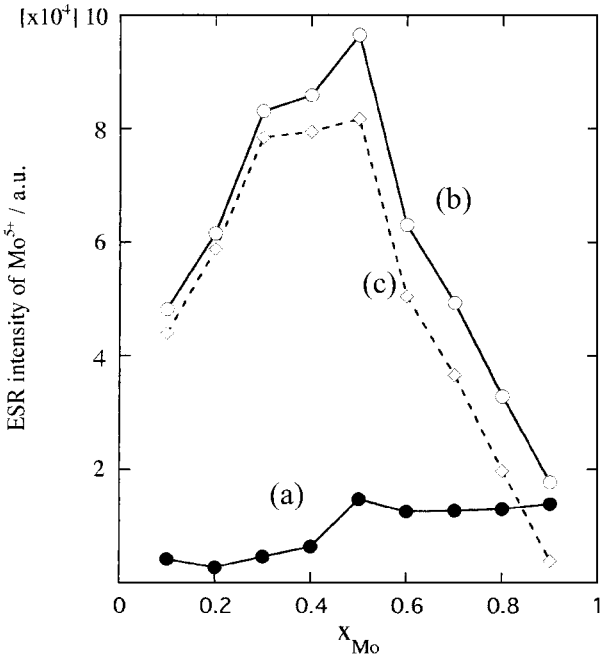

Figure 8 The relative intensity ratio of Mo^{5+} of the (a) unreduced (●) and (b) reduced (○) MoO_3-ZnO oxide (c) (◇) is the difference of (b) and (a).

to be very small. The line shape of (c) is very similar to the increase in I_{ZnMoO3}/I_t as shown in Fig. 5 and to the decrease in I_{ZnMoO4}/I_t of the reduced Mo-Zn oxide. Therefore, the intensity mainly results from the Mo^{5+} species.

3.3. Surface area

SA of ZnO and MoO_3 was 6.1 and 1.5 m^2/g, respectively. SA of the unreduced mixed Mo-Zn oxide was about 7.0 m^2/g at $X_{Mo} \leqq 0.4$ and about 3.0 m^2/g at $X_{Mo} > 0.4$ as shown in Fig. 9. SA of the reduced Mo-Zn oxide increased more than two times of that of the unreduced one and at $X_{Mo} = 0.5$, more than 20 times (70.0 m^2/g). At $X_{Mo} \geqq 0.6$, it kept constant at about 10.0 m^2/g. The (c) in Fig. 9 is the difference obtained by subtracting SA of the unreduced oxide (a) from that of the reduced one (b) and is very similar to that of I_{ZnMoO3}/I_t. This suggests that the change in SA largely depends on the formation of $ZnMoO_3$ by the reduction.

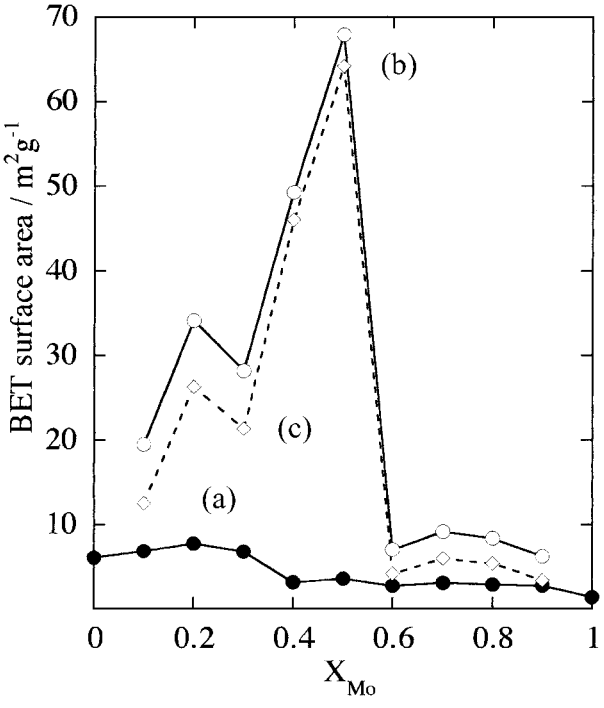

Figure 9 BET Surface Area of the (a) unreduced (●) and (b) reduced (○) MoO_3-ZnO oxide. (c) (◇) is the difference of (b) and (a).

3.4. Mo L_3-edge XANES studies

Fig. 10a shows Mo L_3-edge XANES spectra of MoO_3, $ZnMoO_4$, and MoO_2 as a standard material. For MoO_3, the peak height of the lower energy side is more intense than that of the higher one and, for $ZnMoO_4$, vice versa. The spectrum of MoO_2 is broad and looks like to give a single peak. The energy gap, Δ, which is the difference in the peak-to-peak width between the higher and lower energy sides reflects directly the d orbital splitting. Therefore, Δ is a measure of the ligand field splitting of the final state 4d orbitals. The peak-to-peak width obtained from the second derivative is more precisely than that directly obtained from a XANES spectrum. The second derivative is also shown in Fig. 10b. Δ of MoO_3, $ZnMoO_4$, and MoO_2 obtained from the second derivative was 3.4, 2.4, and 2.5 eV, respectively. It is well known that MoO_3 has an octahedral (MoO_6) unit [Mo^{6+} (d^0)], $ZnMoO_4$, a tetrahedral (MoO_4) one [Mo^{6+} (d^0)], and MoO_2, an octahedral one [Mo^{4+} (d^2)]. According to literatures [21, 35–39], Δ of the octahedral unit is 3.1–4.5 eV and the tetrahedral one, 1.8–2.4 eV. Therefore, the observed Δ of MoO_3 and $ZnMoO_4$ just falls on these ranges. On the other hand, in spite of the symmetry of the MoO_6 octahedron, Δ of MoO_2 is 2.4 eV, which agrees well with the reported value of 2.5 eV [21].

Fig. 11a shows the Mo L_3-edge XANES spectra of the mixed Mo-Zn oxide. The peak height of the higher energy side is more intense than that of the lower one at $X_{Mo} \leqq 0.5$ and at $X_{Mo} \geqq 0.5$, the peak is vice versa. This result suggests that the spectrum consists of at least two components. On the other hand, Fig. 11b shows the spectrum of the reduced Mo-Zn oxide which gives a single like broad line shape, except the spectrum at $X_{Mo} = 0.8$ which is very similar to that of the mixed Mo-Zn oxide at $X_{Mo} = 0.8$.

The second derivatives of the unreduced and reduced Mo-Zn oxide are shown in Fig. 12. For the unreduced oxide, it is clear that at $X_{Mo} \leqq 0.5$ the spectrum consists of one component and at $X_{Mo} = 0.5$, of two components, respectively. While for the reduced one, at $X_{Mo} \leqq 0.5$, the spectrum consists of two components, at $X_{Mo} > 0.6$, of three components, and at $X_{Mo} = 0.8$, two components, respectively. Δ obtained from the second derivatives is summarized in Table I in addition to the values of literatures [21, 35, 39].

4. Discussion

4.1. Surface and/or near the surface structure of the mixed MoO_3-ZnO oxide

We recorded the Mo L_3-edge XANES spectrum in a total electron yield mode, which was constituted by

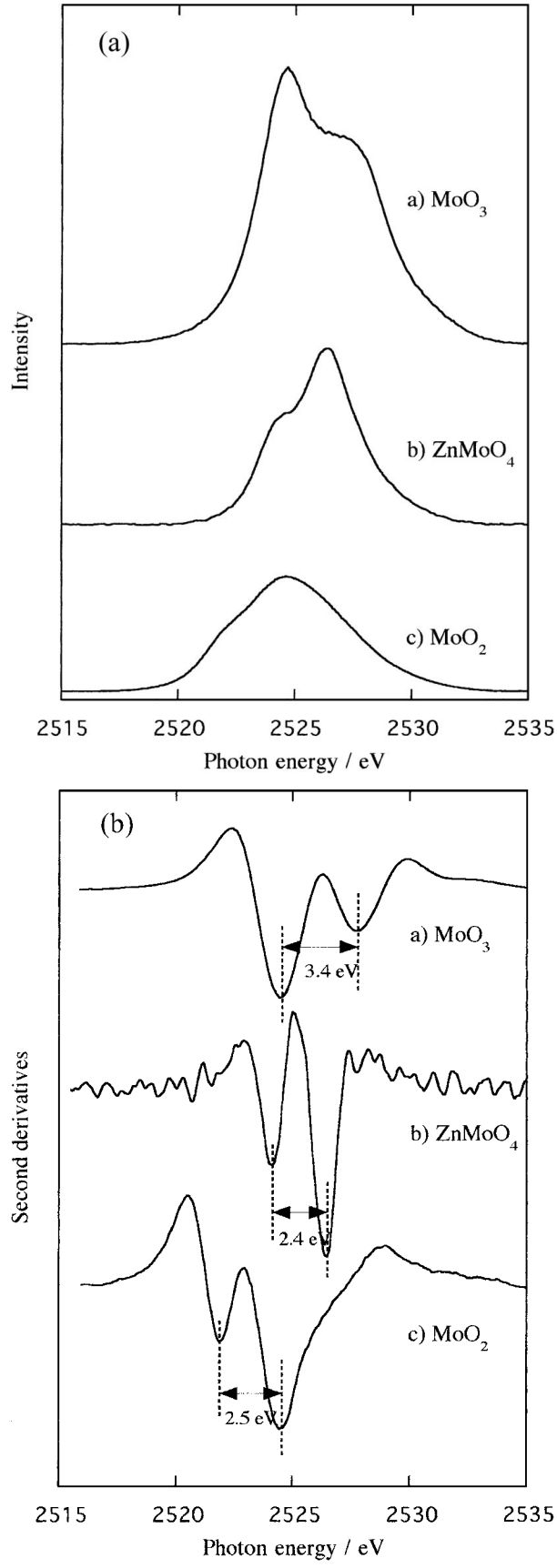

Figure 10 Mo L_3-edge XANES spectra (a) and the second derivatives (b) of standard materials; (a) MoO_3, (b) $ZnMoO_4$, and (c) MoO_2.

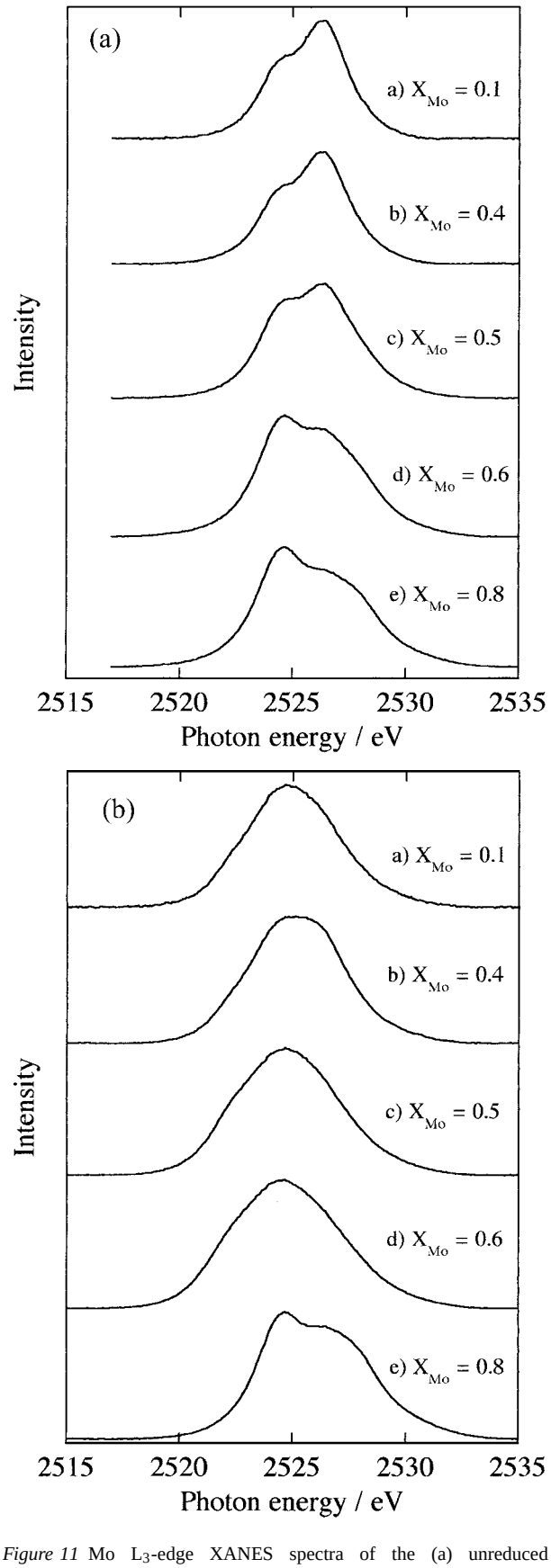

Figure 11 Mo L_3-edge XANES spectra of the (a) unreduced and (b) reduced MoO_3-ZnO oxide (a) $X_{Mo} = 0.1$, (b) $X_{Mo} = 0.4$, (c) $X_{Mo} = 0.5$, (d) $X_{Mo} = 0.6$, and (e) $X_{Mo} = 0.8$.

Auger electrons and low energy secondary electrons [40]. The penetration range into the bulk is possibly several tens angstroms. Therefore, the spectra may reflect the structure of the surface and/or near the surface region. It is well known that Mo atom takes a MoO_6 octahedral coordination and a MoO_4 tetrahedral coordination. MoO_3 gives the typical octahedral coordination. While $ZnMoO_4$ and $ZnMoO_3$ show the tetrahedral

TABLE I The d-orbital splitting, Δ, of the unreduced and reduced MoO_3-ZnO oxide which was obtained from the second derivatives

		d-orbital splitting, Δ/eV		
unreduced	$X_{Mo} = 0.1$		2.2	
	0.4		2.2	
	0.5		2.2	
	0.6		2.2	3.5
	0.8		2.4	3.4
reduced	$X_{Mo} = 0.1$	2.3	1.9	
	0.4	2.2	2.0	
	0.5	2.3	1.8	
	0.6	2.1	2.0	3.5
	0.8		2.4	3.3
$MgMoO_4$	tetrahedral	2.2[21]	1.8[35]	
$PbMoO_4$	tetrahedral	1.9[35]		
Na_2MoO_4	tetrahedral	2.4[21]	2.1[35]	
$ZnMoO_4$	tetrahedral	2.4*		
MoO_3	octahedral	3.4*	3.4[21]	4.0[35]
$HxMoO_3$(H-bronze)	octahedral	3.1-3.2[39]	3.1[21]	
$CoMoO_4$	octahedral	3.3[35]		
$(NH_4)_6Mo_7O_{24}$	octahedral	2.9[21]	3.6[35]	
Ba_2CaMoO_6	octahedral	4.5[35]		
MoO_2	octahedral	2.5*	2.4[21]	

*: present work.

coordination [33, 41]. For MoO_3 with octahedral coordination, the peak height of the lower energy side is more intense than that of the higher one. While for $ZnMoO_4$ with tetrahedral coordination, the peak height of the higher energy side is more intense than that of the lower one. The peaks are attributed to the electron transition from $2p_{3/2}$ to a vacant 4d state; t_{2g} (d_{xy}, d_{xz}, and d_{yz}) and e_g (d_{x2-y2} and d_{z2}) for MoO_3 (octahedral symmetry), and t_2 (d_{xy}, d_{xz}, and d_{yz}) and e (d_{x2-y2} and d_{z2}) for $ZnMoO_4$ (tetrahedral symmetry). The peak heights of the lower and higher energy sides of MoO_3 are therefore different from those of $ZnMoO_4$. This difference in the peak intensity is due to the difference in the transition cross section of the molecular orbital of Mo(4d)-O(2p). Theoretically, the intensity ratio is $t_{2g} : e_g = 3 : 2$ for octahedron and $e : t_2 = 2 : 3$ for tetrahedron. Indeed, MoO_3 gives the octahedral coordination structure and the peak height of the lower energy side is more intense than that of the higher one. $ZnMoO_4$ with the tetrahedral coordination structure gives vice versa. Though MoO_2 has a MoO_6 octahedral symmetry, the spectrum is different from that of MoO_3. The energy gap between t_{2g} and e_g in MoO_2 giving Mo^{4+} ion should be smaller than that giving Mo^{6+} ion, because of the less effect of perturbation by the ligand field of six O ions.

As mentioned above, the spectrum of the Mo-Zn oxide as shown in Fig. 11a consists at least of two components and suggests a superposition of components of Mo ions. Therefore, we can analyze the spectrum of the Mo-Zn oxide by considering the combination of Gaussian and Lorentzian, which consists of octahedral and tetrahedral components. Fig. 13a shows the decomposed curves of the Mo-Zn oxide, which is best fitted by using the synthesized waves of the octahedral and tetrahedral components. The parameters of the decomposed peaks are summarized in Table II. Δ is calculated to be 3.0–3.6 eV for the octahedron and 2.1–2.4 eV for the tetrahedron, which is in good agreement with Δ

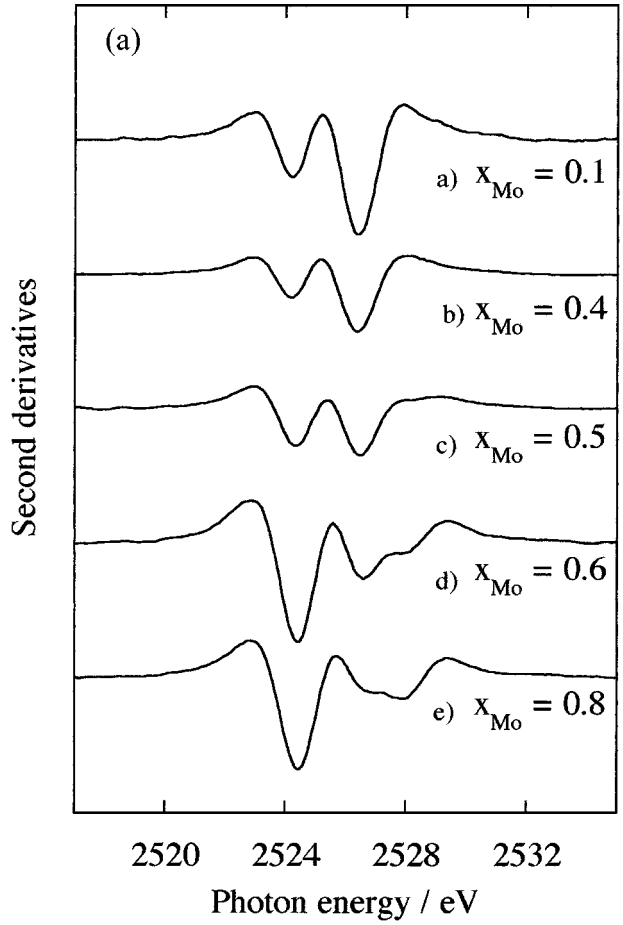

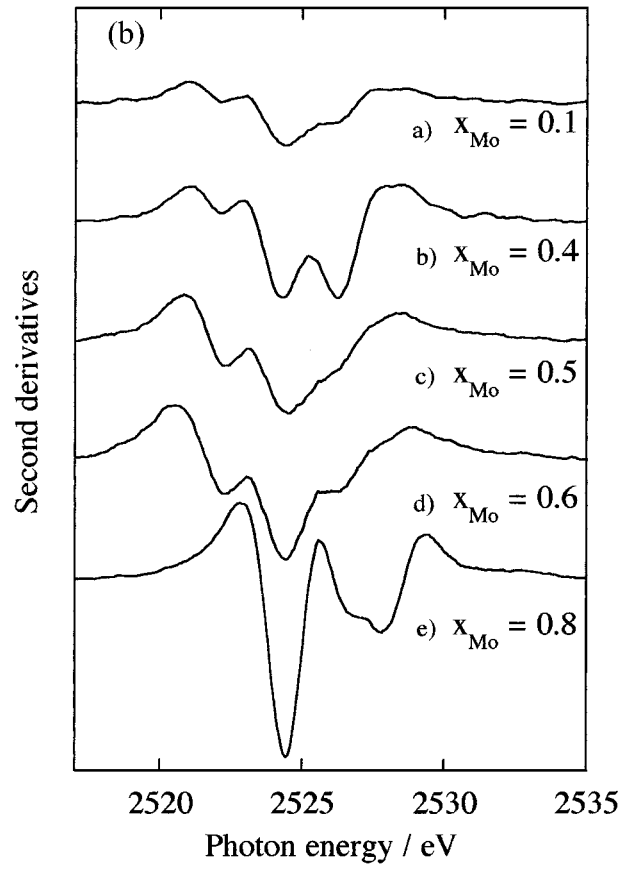

Figure 12 The second derivatives of Mo L_3-edge XANES spectra of the (a) unreduced and (b) reduced MoO_3-ZnO oxide. (a) $X_{Mo} = 0.1$, (b) $X_{Mo} = 0.4$, (c) $X_{Mo} = 0.5$, (d) $X_{Mo} = 0.6$, and (e) $X_{Mo} = 0.8$.

TABLE II The decomposed parameters of XANES spedctra of the unreduced and reduced MoO_3-ZnO oxide

		octahedron			tetrahedron			MoO_2			ratio of area		
		lower	higher/eV	Δ	lower	higher/eV	Δ	lower	higher/eV	Δ	tetra/total	octa/total	MoO_2/total
$ZnMoO_4(Na_2MoO_4)$		—	—	—	2524.1	2526.4	2.3	—	—	—	1.00	0.00	—
MoO_3		2524.5	2527.5	3.0	—	—	—	—	—	—	0.00	1.00	—
unreduced	$X_{Mo}=0.1$	2524.3	2527.7	3.4	2524.3	2526.4	2.1	—	—	—	0.50	0.50	—
	0.4	2524.3	2527.6	3.3	2524.2	2526.3	2.1	—	—	—	0.57	0.43	—
	0.5	2524.4	2527.9	3.5	2524.2	2526.4	2.2	—	—	—	0.64	0.36	—
	0.6	2524.6	2527.7	3.1	2524.1	2526.4	2.3	—	—	—	0.35	0.65	—
	0.8	2524.5	2527.5	3.0	2524.1	2526.4	2.3	—	—	—	0.18	0.82	
reduced	$X_{Mo}=0.1$	2524.5	2527.9	3.4	2524.0	2526.2	2.2	2522.1	2524.0	1.9	0.55	0.25	0.20
	0.4	2524.4	2527.9	3.5	2524.1	2526.3	2.2	2522.1	2524.1	2.0	0.45	0.31	0.24
	0.5	2524.3	2527.8	3.5	2524.0	2526.1	2.1	2522.0	2524.0	2.0	0.38	0.30	0.32
	0.6	2524.2	2527.8	3.6	2524.0	2526.1	2.1	2521.9	2523.9	2.0	0.36	0.33	0.31
	0.8	2524.6	2527.6	3.0	2524.0	2526.4	2.4	—	—	—	0.20	0.80	—

obtained from the second derivative curves. The ratio of each component vs the total component also is calculated as shown in Table II and in Fig. 14. This gives the surface or near the surface structure. According to the results, at $X_{Mo} \leqq 0.5$, $ZnMoO_4$ is dominant on the surface, while at $X_{Mo} > 0.5$, MoO_3, dominant. This indicates that the surface structure is largely different from the bulk structure.

On the other hand, the XANES spectrum of the reduced Mo-Zn oxide is remarkably broad and simple except the spectrum of $X_{Mo} = 0.8$. Therefore, it is difficult to clarify the d-orbital splitting. XRD results show the presence of MoO_3, $ZnMoO_4$, $ZnMoO_3$ and MoO_2. The XANES spectrum, therefore, may consist at least of two or three components. We also tried to simulate the spectrum of the reduced Mo-Zn oxide by considering the octahedral, the tetrahedral, and the MoO_2 components. The decomposed spectra are well fitted as shown in Fig. 13b. The spectrum of $X_{Mo} = 0.8$ has clear two peaks and the decomposed spectrum consists of two component as well as that of the unreduced Mo-Zn oxide of $X_{Mo} = 0.8$. The parameters of the decomposed peaks and the calculated ratio of each component vs the total component is also shown in Table II and in Fig. 14, show the presence of MoO_2 even at low X_{Mo}. This suggests that MoO_2 is also formed at low X_{Mo} on the surface by reduction, even though MoO_2 was only detected at $X_{Mo} > 0.4$. At $X_{Mo} \leqq 0.5$ MoO_3 keeps nearly constant value on the surface, but at $X_{Mo} > 0.5$ MoO_3 become dominantly. XANES results are different from XRD results. This means that the surface structure differs extensively from the bulk structure. It is expected that this difference may produce a new function for catalytic reaction.

4.2. Solid phase reaction between MoO_3 and ZnO heated in air

If the reaction between MoO_3 and ZnO proceeds stoichiometrically to produce $ZnMoO_4$, the change in theoretical intensity of each component can be calculated as shown by a dotted line in Fig. 3. At $X_{Mo} < 0.5$ the change in I_{ZnMoO4}/I_t and I_{ZnO}/I_t is very similar to that of the theoretical ones except at $X_{Mo} = 0.1$. At $X_{Mo} \geqq 0.5$ the observed each component shows a different behavior with that of the theoretical one. I_{ZnO}/I_t gradually decreases to 0 at $X_{Mo} = 1$ and I_{ZnMoO4}/I_t is small compared with the theoretical one. I_{MoO3}/I_t is larger than that of the theoretical one. This means that at $X_{Mo} \geqq 0.5$ the reaction between MoO_3 and ZnO does not take place completely.

As shown in Fig. 9, SA of ZnO is 6.1 m^2g^{-1} and that of MoO_3, 1.4 m^2g^{-1}. When ZnO is impregnated in an ammonium molybdate solution a desired amount of molybdenum is loaded on or covers ZnO. SA of the sample at $X_{Mo} \leqq 0.3$ is very similar to that of ZnO, while at $X_{Mo} \geqq 0.4$ SA is close to that of MoO_3. This suggests that the designed amount of molybdenum is loaded theoretically on ZnO. XRD, ESR, and BET results show the change in their behavior at $X_{Mo} = 0.4$. When the impregnated sample is heated in air at $X_{Mo} \leqq 0.4$, the ammonium molybdate (denoted as AMMo) is at first oxidized to MoO_3 and the reaction between MoO_3 and ZnO takes place stoichometrically within 1 h to give $ZnMoO_4$. On the other hand, at $X_{Mo} > 0.4$, AMMo loaded thick on ZnO is oxidized by calcination to MoO_3. The MoO_3 layer increases in thickness with the increase in X_{MoO3}, of which SA is very similar to that of MoO_3. In this case, when an adequate thickness layer of $ZnMoO_4$ is produced, the further reaction is difficult to take place. In order to proceed further reaction to give $ZnMoO_4$, Mo and/or Zn ions should diffuse through the $ZnMoO_4$ layer. But no large change in XRD pattern was observed though the Mo-Zn oxide was calcined for 5 h. Therefore, the diffusion should be very slow to give $ZnMoO_4$. It is reasonable to conclude as follows; (1) When MoO_3 is loaded on ZnO as an island or covers by a thin MoO_3 layer, which directly contacts to ZnO, the reaction between MoO_3 and ZnO takes place easily to give $ZnMoO_4$. (2) In the case of heavy coverage of MoO_3 on ZnO, when an adequate amount of $ZnMoO_4$ is formed between the MoO_3 and ZnO layers, the further reaction is difficult to occur, because of no direct contact between MoO_3 and ZnO and/or of no easy diffusion of Mo and/or Zn ions. Those can be illustrated as the model in Fig. 15.

4.3. Formation of $ZnMoO_3$ and MoO_2

XRD result of the reduced Mo-Zn oxide is different from that of the unreduced Mo-Zn oxide. As mentioned above, a new product of $ZnMoO_3$

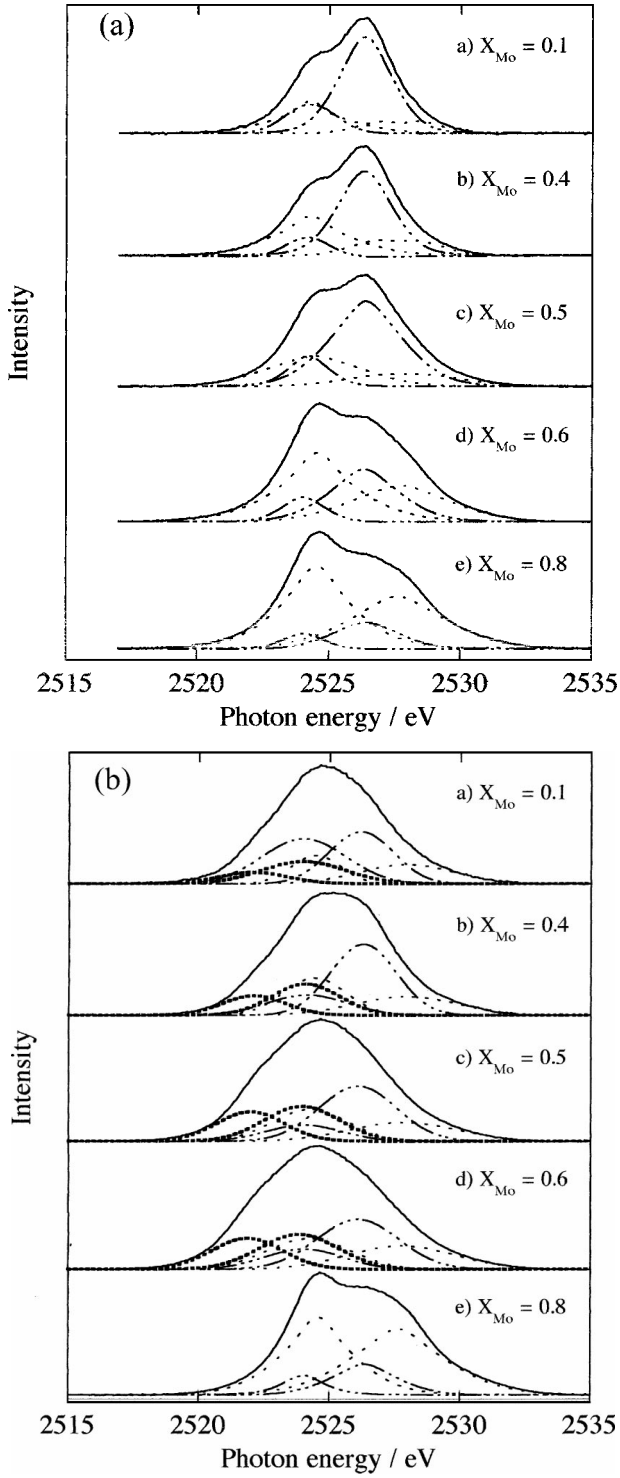

Figure 13 The decomposed curves of Mo L_3-edge XANES spectra of the (a) unreduced and (b) reduced MoO_3-ZnO oxide. ——: the observed spectrum. — — — —: tetra coordination, – – – –: octa coordination, and – – – – –: MoO_2.

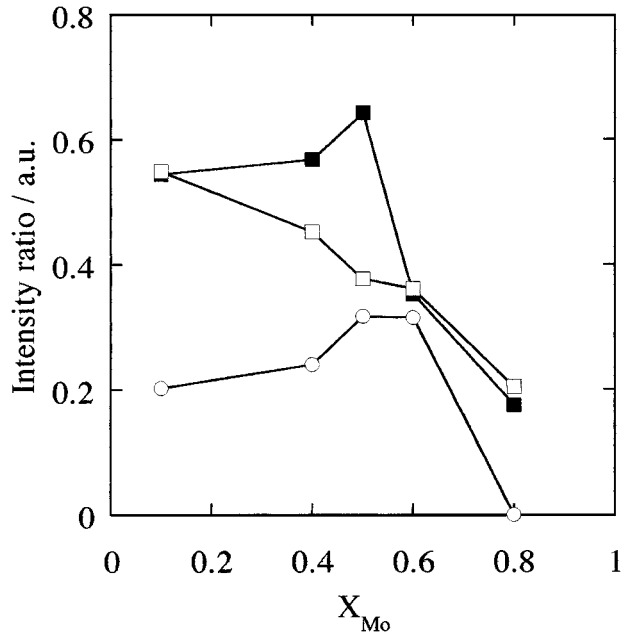

Figure 14 The intensity ratio of surface component calculated from the decomposed spectrum; (a) tetrahedral Mo component of the unreduced oxide (■) and reduced one (□), (b) octahedral Mo component of the unreduced oxide (▲) and reduced one (△), and (c)MoO_2 component of the reduced oxide (◇).

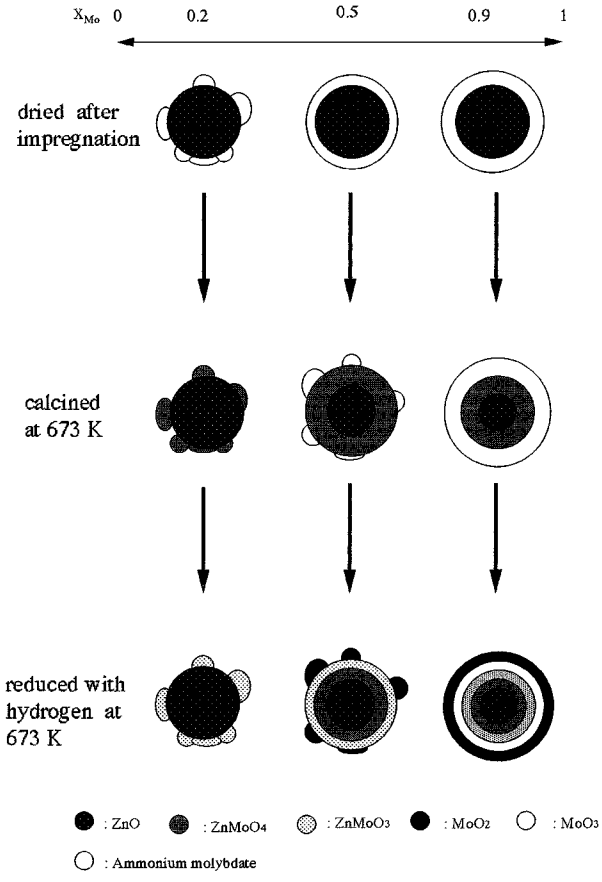

Figure 15 Model of the mixed MoO_3-ZnO oxide.

and MoO_2 appeared. According to Manthiram and Gopalakrishnan [33], $ZnMoO_3$ is a cubic crystal and gives the defect spinel structure with an anion vacancy like $Zn[Mo_{4/3}Zn_{1/3}\square_{1/3}]O_4$, where □ represents the vacancy. It can be written as $ZnO[Mo_{4/3}Zn_{1/3}\square_{1/3}]O_3$ or $(4/3)(ZnMo\square_{1/4}O_3)$. $ZnMoO_3$ with the vacancy should give Mo^{5+} species. Indeed, according to ESR results, $ZnMoO_3$ and the reduced Mo-Zn oxide give the strong signal due to Mo^{5+} and the lattice defects like the anion vacancy [26–29]. Fig. 16 shows the change in SA, I_{ZnMoO3}/I_t and the intensity of Mo^{5+} of the reduced Mo-Zn oxide. This change in SA is very similar to that in I_{ZnMoO3}/I_t. It suggests that the increase in SA results from the formation of $ZnMoO_3$ with the anion vacancy. When $ZnMoO_3$ begins to appear by the reduction a

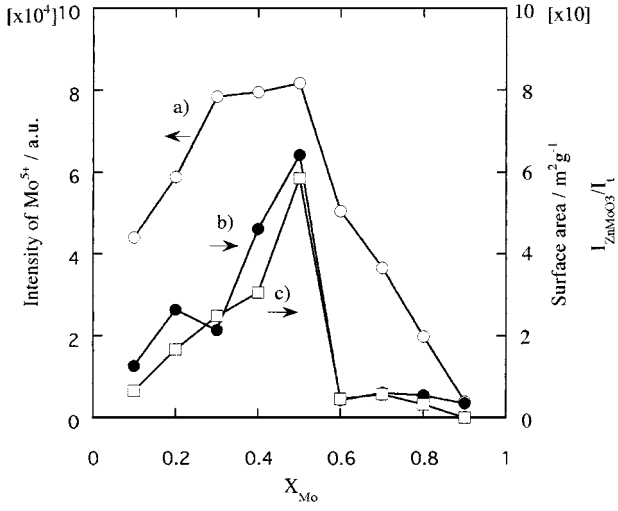

Figure 16 The change in SA, I_{ZnMoO3}/I_t, and the intensity of Mo^{5+} against X_{Mo}.

distortion is produced in the structure of $ZnMoO_4$ and Mo^{5+} is also formed. Therefore, the intensity of Mo^{5+} increases with the formation of $ZnMoO_3$. On the other hand, at $X_{Mo} = 0.5$ MoO_2 begins to appear. $ZnMoO_3$ decreases and $ZnMoO_4$ appears at $X_{Mo} \geqq 0.6$. These results mean that a part of MoO_3 is reduced to MoO_2 and $ZnMoO_4$ is difficult to be reduced, though a very small amount of $ZnMoO_3$ is formed. SA decreases steeply at $X_{Mo} = 0.6$, which corresponds to that of MoO_3. The intensity of Mo^{5+} decreases gradually, which may result from the distortion of the $ZnMoO_4$ structure and the formation of MoO_2.

At $X_{Mo} \leqq 0.4$, $ZnMoO_4$ covered thinly on ZnO is easy to be reduced to $ZnMoO_3$, because of direct contact with hydrogen. While, at $X_{Mo} \geqq 0.5$, a small amount of ZnO is wrapped with the $ZnMoO_4$ layer, which is covered with the thick MoO_3 layer. In this case, MoO_3 is easy to be reduced to MoO_2. In order to reduce to $ZnMoO_3$, it is necessary for $ZnMoO_4$ to contact directly with hydrogen. In the help of Pt on MoO_3, hydrogen should diffuse easily through the MoO_3 layer, but it is difficult to diffuse in this reaction condition. Therefore, in this region, MoO_3 is easily reduced to MoO_2, but $ZnMoO_4$ is difficult to be reduced. Considering above results and discussion, we can conclude that at $X_{Mo} \leqq 0.4$, $ZnMoO_4$ is easily reduced to $ZnMoO_3$ and at $X_{Mo} > 0.5$ MoO_3 is easy to be reduced to MoO_2. However, at $X_{Mo} \geqq 0.6$ $ZnMoO_4$ is difficult to be reduced. We have proposed the model as illustrated in Fig. 15. However, it needs another precise and direct observation by using another kinds of instruments.

5. Conclusion

(1) When the mixed Mo-Zn oxide is calcined in air, the solid phase reaction takes place easily like as $ZnO + MoO_3 \rightarrow ZnMoO_4$, but at $X_{Mo} > 0.5$ the further reaction to $ZnMoO_4$ is little difficult, because the diffusion of Mo and/or Zn ions is not so easy.

(2) By the reduction with hydrogen at $X_{Mo} \leqq 0.5$ $ZnMoO_4$ is reduced to $ZnMoO_3$ with the anion vacancy, which gives the increase in SA and in the amount of Mo^{5+}. At $X_{Mo} > 0.5$ the reaction proceeds as $ZnO[Mo_{4/3}Zn_{1/3}\square_{1/3}]O_3 + MoO_3 \rightarrow ZnMoO_4 + MoO_2$.

(3) The surface and/or near the surface structure is very different from the bulk structure. MoO_2 appears on the surface at low X_{Mo}, but does at $X_{Mo} > 0.4$ in the bulk.

References

1. J. HABER, "The Role of Molybdenum in Catalysis" (Climax Molybdenum Co., Ann Arbor, MI, 1981).
2. K. SEGAWA and I. E. WACHS, in "Characterization of Catalytic Materials," edited I. E. Wachs (Buterworth-Heinemann, Boston, 1992) p. 72.
3. J. R. BARTLETT and R. P. COONEY, in "Spectroscopy of Inorganic-Based Materials," edited by R. J. H. Clark and R. E. Hester (John Wiley and Sons, New York, 1987) p. 187.
4. O. H. HAN, C. Y. LIN, N. SUSTACHE, M. MCMILLAN, J. D. CARRUTHERS, K. W. ZILM and G. L. HALLER, *Appl. Catal. A: Gen.* **98** (1993) 195.
5. J. M. STENCEL, "Raman Spectroscopy for Catalysis" (Van Norstrand Reinhold, New York, 1990) p. 51.
6. J. MEDEMA, C. VON STAM, V. H. J. DE BEER, A. J. A. KONINGS and D. C. KONINGSBERGER, *J. Catal.* **53** (1978) 386.
7. C. C. WILLIAMS, J. G. EKERDT, J.-M. JEHNG, F. D. HARDCASTLE and I. E. WACHS, *J. Phys. Chem.* **95** (1991) 8791.
8. L. RODRIGO, K. MARCINKOWSKA, A. ADNOT, P. C. ROBERGE, S. K. KALIAGUINE, J. M. STENCEL, L. E. MAKOVSKY and J. R. DIEHE, *ibid.* **90** (1986) 2670.
9. A. K. DATTA, J. W. HA and J. W. REGALBUTO, *J. Catal.* **133** (1992) 55.
10. N. SPANOS, H. K. MATRALIS, C. KORDULIS and A. LYCOUROGHIOTIS, *ibid.* **136** (1992) 432.
11. T. MACHEJ, J. HABER, A. M. TUREK and T. E. WACHS, *Appl. Catal.* **70** (1991) 115.
12. T. ONO, H. MIYATA and K. KUBOKAWA, *J. Chem. Soc. Faraday Trans. I* **83** (1987) 176.
13. H. MIYATA, S. TOKUDA, T. ONO, T. OHNO and F. HATAYAMA, *ibid.* **86** (1990) 229.
14. C. MORTERA, A. ZECCHINA and G. COSTA (eds.), "Structure of Surface" (Elsevier, Amsterudam, 1989) p. 525.
15. J.-M. JEHUG, A. M. TUREK and I. E. WACHS, *Appl. Catal. A: Gen.* **83** (1992) 179.
16. H. HU, I. E. WACHS and S. R. BARE, *J. Phys. Chem.* **99** (1995) 10897.
17. G. DEO and I. E. WACHS, *ibid.* **95** (1991) 5889.
18. GIL-LLAMBIAS, *J. Catal.* **135** (1992) 1.
19. A. NISHIYAMA, N. KOSUGI and H. KURODA, *ibid.* **135** (1992) 746.
20. H. ARITANI, T. TANAKA, T. FUNABIKI, S. YOSHIDA, M. KUDO and S. HASEGAWA, *J. Phys. Chem.* **100** (1996) 5440.
21. H. ARITANI, T. TANAKA, T. FUNABIKI, S. YOSHIDA, N. SOTANI, K. EDA and S. HASEGAWA, *ibid.* **100** (1996) 19495.
22. R. J. KOKES, *ibid.* **66** (1962) 99.
23. H. SALTSBURG and D. P. SNOWDEN, *ibid.* **68** (1964) 2734.
24. K. M. SAUCIER and T. FREUND, *J. Catal.* **3** (1964) 293.
25. K. NAKAMURA, K. EDA and N. SOTANI, *Applied Catalysis A, Gene.* **178** (1999) 167.
26. M. CHE, F. FIGUERAS, M. FORISSIER, J. C. MCATEER, M. PERRIN, J. I. PORTEFAIX and H. PRALIAUD, in Proceedings VIth Int. Congr. Catal. (The Chemical Society, London, 1977) Vol. I, p. 261.
27. R. F. HOWE and I. R. LEITH, *J. Chem. Soc. Faraday Trans. I* **69** (1973) 1967.
28. C. LOUIS and M. CHE, *J. Phys. Chem.* **91** (1987) 2875.
29. A. LATEF, C. F. AISSI and M. GUELTON, *J. Catal.* **119** (1989) 368.
30. M. CODELL and H. GISSER, *J. Phys. Chem.* **72** (1968) 2460.

31. J. H. LUNSFORD and J. P. JAYNE, *ibid.* **44** (1966) 1487.
32. K. HOFFMANN and D. HAHN, *Phys. Stat. Sol. (a)* **24** (1974) 637.
33. A. MANTHIRAM and J. GOPALAKRISHNAN, *Mat. Res. Bull.* **15** (1980) 207.
34. K. DYREK and M. LABANOWSKA, *J. Chem. Soc. Faraday Trans.* **87** (1991) 1003.
35. J. EVANS, W. FREDERICK and W. MOSSELMANS, *J. Phys. Chem.* **95** (1991) 9673.
36. G. N. GEORGE, W. E. CLELAND, J. H. ENEMARK, B. E. SMITH, C. A. KIPKE, S. A. ROBERTS and S. P. CRAMER, *J. Amer. Chem. Soc.* **112** (1990) 2541.
37. H. HU, I. E. WACHS and S. R. BARE, *J. Phys. Chem.* **99** (1995) 10897.
38. S. R. BARE, G. E. MITCHELL, J. J. MAJ, G. E. VRIELAND and J. L. GLAND, *ibid.* **97** (1993) 6048.
39. K. NAKAMURA, K. EDA and N. SOTANI, *Bull. Chem. Soc. Jpn.* **71** (1998) 2063.
40. A. ERBIL, G. S. CARGILL, R. FRAHM and R. F. BOEHME, *Phys. Rev. B* **37** (1988) 2450.
41. S. C. ABRAHAMS, *J. Chem. Phys.* **46** (1967) 2052.

Received 26 August 1999
and accepted 22 February 2000